frontiers | Frontiers in Materials

TYPE Original Research
PUBLISHED 24 January 2024
DOI 10.3389/fmats.2023.1341006

OPEN ACCESS

EDITED BY
Bernardo Mendoza,
Centro de Investigaciones en Optica, Mexico

REVIEWED BY
Preeti Gupta,
Leibniz Institute for Solid State and Materials Research Dresden (IFW Dresden), Germany
Ramon Carriles,
Centro de Investigaciones en Optica, Mexico

*CORRESPONDENCE
Weitian Wang,
wtwang@ytu.edu.cn

RECEIVED 19 November 2023
ACCEPTED 27 December 2023
PUBLISHED 24 January 2024

CITATION
Huang Z, Ma Q, Wang D, Zhao R, Niu R and Wang W (2024), The band gap and nonlinear optical susceptibility of $SrSn_{1-x}V_xO_3$ films. *Front. Mater.* 10:1341006.
doi: 10.3389/fmats.2023.1341006

The band gap and nonlinear optical susceptibility of $SrSn_{1-x}V_xO_3$ films

Ziheng Huang, Qiushuang Ma, Depeng Wang, Rongjing Zhao, Ruifeng Niu and Weitian Wang*

School of Physics and Electronic Information, Yantai University, Yantai, China

Perovskite-type oxide $SrSn_{1-x}V_xO_3$ thin films with different concentrations x = 0.1–0.9 were fabricated by using pulsed-laser deposition, and the effects of V doping on the structure, optical band gap and the third-order optical nonlinearity were systematically investigated. With the increase of x value, the lattice parameters of $SrSn_{1-x}V_xO_3$ decrease from 3.997 to 3.862 Å gradually, while the optical band gaps firstly increase and then decrease with boundary at x = 0.3. The third-order nonlinear optical responses were studied via the z-scan technique. The closed-aperture measurements show a negative nonlinear refractive index n_2, and the open-aperture measurements demonstrate a saturable absorption β. Both the n_2 and β responses vary with the increase of V doping level. The metal-oxygen chemical bond along with the localized $V^{5+}Sn^{2+}V^{5+}$ complex contribute to the enhancement of optical nonlinearity, and the highest value of third-order susceptibility $\chi^{(3)}$ is observed in $SrSn_{0.5}V_{0.5}O_3$ film.

KEYWORDS

nonlinear optical properties, band gap, thin films, pulsed-laser deposition, perovskite

1 Introduction

With the rapid development of optoelectronic science and technology, multifunctional devices with modulated performance have attracted worldwide research attention (Benaissa et al., 2021; Leal-Perez et al., 2022). Lead-free perovskite ABO_3-structured oxides are promising optoelectronic materials due to their noticeable ferroelectric, piezoelectric, optical nonlinearity, best compatibility and environment-friendly characteristics (Pattipaka et al., 2019; Guo et al., 2022). Therefore, theoretical research and experimental explorations in the generation mechanism of optical nonlinearity and properties modulation have been intensively studied in the past decade and have made a great progress especially through A-site or B-site ion-doping (Sakhya, et al., 2017; Absike et al., 2022; Shereef et al., 2023; Wang et al., 2023).

Perovskite-structured $SrSnO_3$ (SSO) is a remarkable material among the family of alkaline earth stannates. Due to the high transparency, thermal stability, semiconductor nature (band gap: 4.24 eV), $SrSnO_3$ shows promising applications in photovoltaic equipment which highlights excellent optical and electrical properties (Gao et al., 2016). Moreover, $SrSnO_3$ can be used as a chemically stable matrix for A-site or B-site ion-doping to study the optical band gap modulation and linear or nonlinear optical properties. Based on theoretical analysis and experimental results, the doped $SrSnO_3$ materials have shown much better optical and electrical properties, and various metal dopants such as Co, Nb, Ta, Fe have been

chosen for the desired qualities (Liu et al., 2014; Liu et al., 2017; Gao et al., 2019; Li et al., 2020).

As is known, the selection of an appropriate dopant is important for modulating the optical and electrical properties of doping matrix. Vanadium (V) is a multivalent element, and vanadium oxide has a large third-order nonlinear optical response among transition-metal oxides (Ando et al., 1995). Recently, it has been reported that transparent $SrVO_3$ (SVO) has a cubic perovskite structure with a band gap of approximately 3.1 eV (Oka et al., 2020). Taken into consideration of the matrix and dopant, doping V into $SrSnO_3$ may result in an enhanced optical nonlinearity and a modulated optical band gap.

In this study, we report the fabrication of a series of V-doped $SrSnO_3$ epitaxial films ($SrSn_{1-x}V_xO_3$, $x = 0.1–0.9$) on MgO substrates by using pulsed laser deposition (PLD) technique. The doping effect on modulation of the band gap and enhancement of the third-order optical nonlinearity was investigated.

2 Experimental details

$SrSn_{1-x}V_xO_3$ films were deposited on (001)-oriented MgO single-crystal substrates by using PLD employing a Lambda Physic KrF excimer laser with a pulse width of 20 ns operating at a repetition frequency of 4 Hz. The ceramic targets were synthesized through high-temperature solid-state reaction using $SrCO_3$, SnO_2, and V_2O_5 powders (Macklin Chemical Co. Ltd., 99.95%) as raw materials with desirable molar ratio. In this experiment, five samples were prepared with setting x = 0.1, 0.3, 0.5, 0.7, and 0.9, and the corresponding deposited films were denoted as SSVO1, SSVO3, SSVO5, SSVO7, and SSVO9, respectively. Prior to deposition, the chamber was vacuumed to a base pressure of 1.0×10^{-4} Pa, and the distance between the target and the substrate was set as 35 mm. During the process of deposition, the films were deposited at 750°C under an oxygen pressure of 30 Pa. A growth rate monitor was used to control the thickness of the fabricated films to be about 180 nm. The *in-situ* annealing after deposition was carried out for 20 min in the same oxygen ambient in order to obtain better uniformity and crystallinity for the subsequent optical measurements.

The crystal structure and orientation of the prepared samples was characterized by x-ray diffractometer (XRD, Bruker D8-A25) using Cu-Kα radiation with a Ni filter. X-ray photoelectron spectroscopy (XPS, VGESCALab-5) equipped with a source of Mg-Kα exciting radiation was used to study the chemical state changes with doping concentration. The optical absorption spectra in the wavelength range of 300–800 nm were used to determine the optical band gap modulation.

The third-order optical nonlinearity was investigated by using the z-scan technique (Bahae et al., 1990). The optical schematic diagram is shown in Figure 1. The incident beam source was a picosecond laser operating at λ = 532 nm. The focal length of the converging lens was f' = 12 cm, and the beam waist radius was about 30 μm at the focal point. Beam splitter 1 and Detector 1 were used to monitor the fluctuation of pulse laser energy. The open-aperture (OA) and closed-aperture (CA) measurements were carried out by Detector 2 and Detector 3, respectively. Detailed parameters of z-scan experiment used for the calculation of third-order nonlinearity are listed in Table 1.

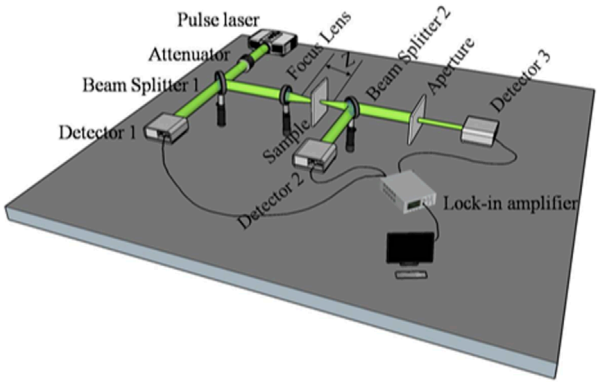

FIGURE 1
Typical setup of the z-scan experiment.

TABLE 1 Parameters of z-scan experiment.

Parameters	Value
Laser wavelength λ	532 nm
Focal length f'	12 cm
Beam waist ω_0	30 μm
Laser power I_0	5.0 MW cm^{-2}
Pulse duration	30 Ps
Repetition rate	10 Hz

3 Results and discussion

Figure 2A presents the XRD profiles of the deposited SSVO films on MgO (001) substrates in the range of 20–50°. It can be seen that besides the diffraction peaks from the MgO substrate, only sharp (00*L*) peaks of the SSVO films are observed, and no visible impurity phase can be detected, which suggests that all the samples are grown with a preferred *c*-axis orientation. The full width at half-maximum (FWHM) of the x-ray rocking curve from the (002) peak of deposited films is in the range of 0.21°–0.69°, as shown in the inset of Figure 2A, indicating the good crystallinity of the films. Typical x-ray φ scans around the (101) peak of SSVO3 film and MgO (112) peak were shown in Figure 2B. The four-fold symmetry with 90° intervals suggests the epitaxial in-plane texture between the films and the underlying substrate.

As is known, the lattice parameter of pseudocubic-structured SSO is 4.082 Å (Zhang et al., 2006), while that of cubic SVO is 3.843 Å (Makino et al., 1998), indicating the predictable lattice matching between the SSVO films and the cubic MgO substrates (4.13 Å). As shown in Figure 2A, the location of (00*L*) peaks of the SSVO films shift to the high-angle direction with the increase doping concentration of V, which implies a decrease of lattice constant *c*. The variation of the calculated value of *c* with *x* in $SrSn_{1-x}V_xO_3$ is shown in Figure 2C. The lattice constant decreases from 3.997 Å for SSVO1 to 3.862 Å for SSVO9. As is known, the size of Sn^{4+} ion is 0.69 Å,

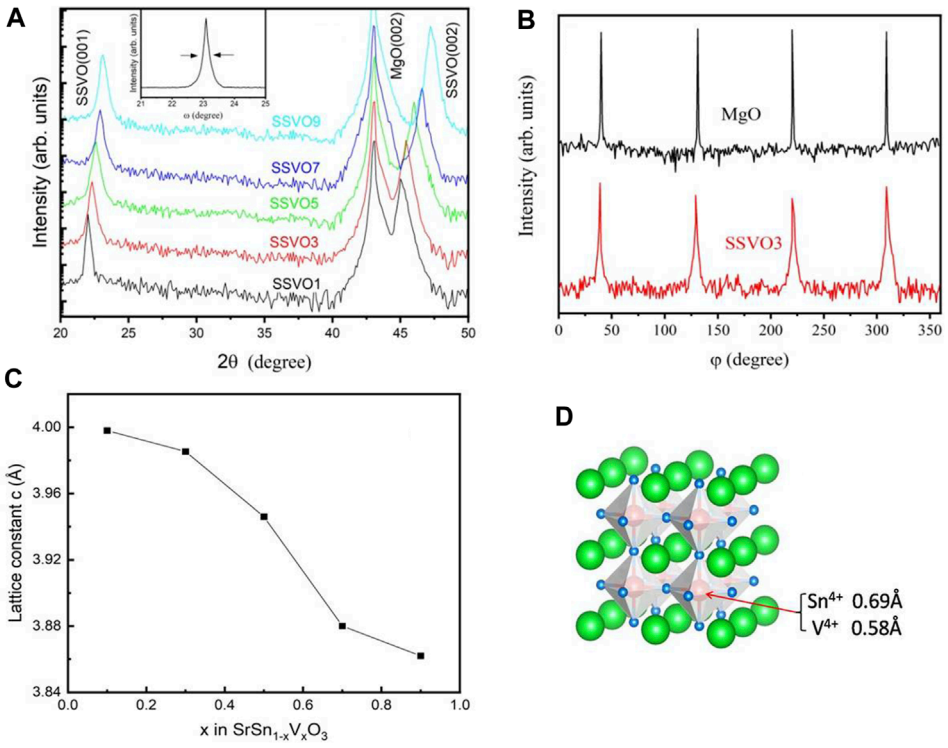

FIGURE 2
(A) XRD profiles of the prepared SSVO samples. Inset: ω-scan rocking curve on the SSVO3 (002) peak. **(B)** φ-scan patterns of the (101) peak of SSVO3 film and MgO substrate around (112) reflection. **(C)** The lattice constant *c* for the prepared samples as a function of V concentration. **(D)** The schematic display of SSVO atomic structure.

while that of V^{4+} is 0.58 Å. Doping with smaller ions is responsible for the decreased lattice constant. The schematic display of SSVO atomic structure is illustrated in Figure 2D.

XPS data were recorded to investigate the valence states of the chemical elements for the films, and the C 1s peak at 284.8 eV was used as a standard reference. Figures 3A–C show the binding energies of Sr 3d, Sn 3d, V 2p + O 1 s for the films, respectively. The Sr 3d spectra are approximately the same within the V doping concentrations, indicating that the doping ions have almost no influence upon the chemical state of Sr ions. Typical Sr 3d spectra for SSVO3, as shown in Figure 3D, comprise a doublet located at 133.80 eV and 132.25 eV, respectively. The binding energies can be assigned to Sr 3d3/2 and Sr 3d5/2, suggesting the existing Sr^{2+} state in the samples.

Figure 3B depicts two peaks of Sn 3d photoelectron spectra. The broad binding energy of Sn 3d5/2 at low doping concentrations ($x \leq 5$) implies multivalent Sn ion in the films. For clarity, Sn 3d spectra for SSVO3 are shown separately in Figure 3E. By using the method mentioned within the literature (Silversmit et al., 2004; Biesinger et al., 2010), the Sn 3d5/2 data break down into two peaks located at 486.10 eV (blue) and 486.95 eV (red), which corresponds to Sn^{2+} and Sn^{4+} oxide states, respectively. As is known, the electronegativity value of Sn element is 1.8, while that of V element is 1.6. Doping with a lower electronegativity element is responsible for the observed low oxidation state Sn^{2+} in the SSVO films. With the increase of doping concentration *x*, however, the Sn 3d5/2 peak becomes sharper and centers at 486.95 eV, as shown in Figure 3B. This analysis indicates that most of the Sn ion in SSVO shows + 4 states at high doping concentration of V ($x > 5$).

Figure 3C presents the binding energies of V 2p + O 1s targeted region. The V 2p3/2 peak shifts toward lower binding energies with increasing V content in SSVO films, indicating the reduced V oxide state. Generally, the V element exhibits multiple chemical valences in the family of vanadium oxides, such as +2, +3, +4, +5 valences. However, V^{5+} is the most stable state in V-O oxide system (Atuchin et al., 2008). Detailed analysis of V 2p + O 1s states is shown in Figure 3F. The asymmetric V 2p3/2 binding energy is deconvoluted into three peaks located at 515.86 (dark yellow), 516.88 (magenta), and 517.71 eV (cyan), corresponding to +3, +4, +5 states of V ions, respectively. With the increase doping concentration of V, the V 2p3/2 peak shifts to the lower energy side and centers at 516.88 eV, as shown in Figure 3C. The V^{4+} oxide state is consistent with the observed Sn^{4+} state in Figure 2B at $x > 5$, which is the requirement of the charge balance.

The O 1s signal of SVVO3 is also shown in Figure 3F, which can be resolved into three peaks centered at 529.8 (blue), 530.7 (red), and 531.8 eV (green), respectively. The peak located at the lowest binding energy can be attributed to the lattice oxygen of the SSVO films, while the other two peaks at higher binding energies are possibly related with the organic surface contamination or physisorbed species (Manorama et al., 2001; Sharma et al., 2005).

Optical bandgap (E_g) of transparent perovskite-structured oxides is sensitive to the dopants. For SSVO films as a direct

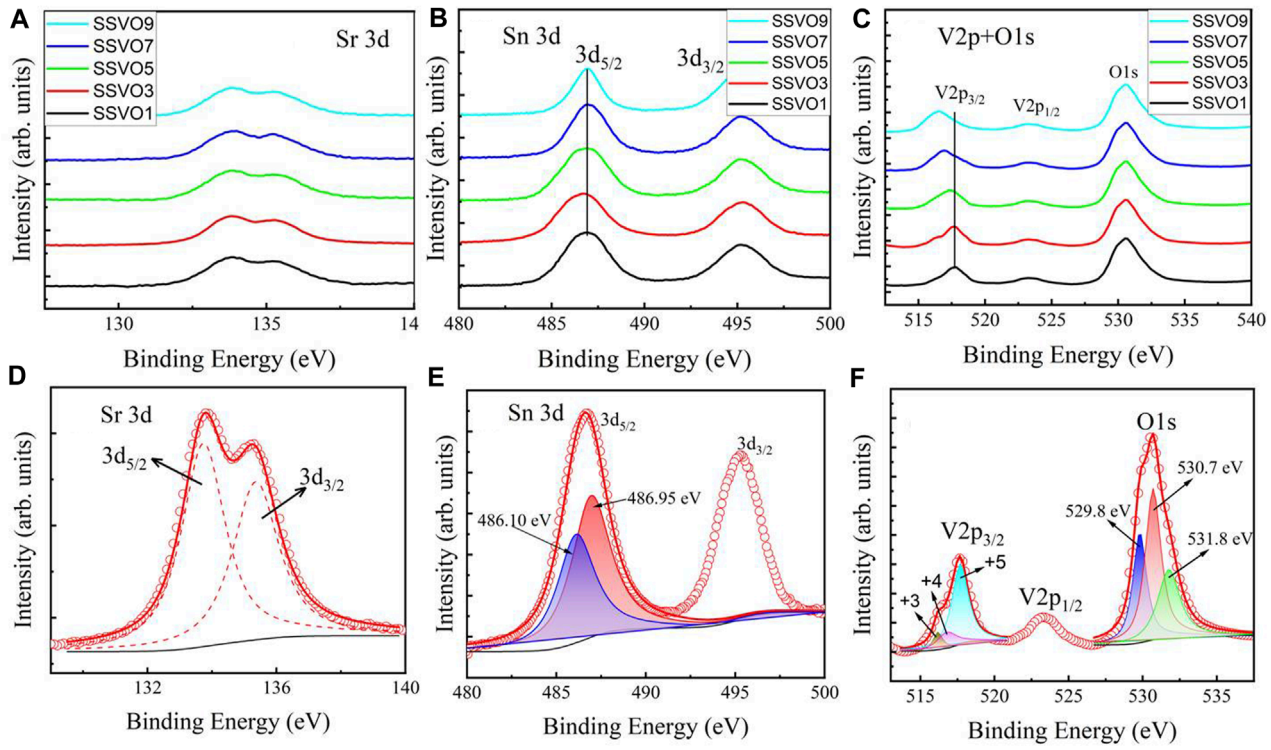

FIGURE 3
XPS spectra of **(A)** Sr 3d, **(B)** Sn 3d, and **(C)** V 2p + O 1s for the prepared SSVO films. Deconvolution of **(D)** Sr 3d, **(E)** Sn 3d, and **(F)** V 2p + O 1s spectra for typical SSVO3 sample.

semiconductor, E_g can be determined by using the Tauc's equation (Tauc et al., 1966)

$$(\alpha h\nu)^2 = A\left(h\nu - E_g\right)$$

where α is the optical linear absorption coefficient, $h\nu$ is the applied photon energy in eV, and A is a constant coefficient.

The relationship between $(\alpha h\nu)^2$ and $h\nu$ is plotted in Figure 4. By linear extrapolating the curves to $(\alpha h\nu)^2 = 0$, E_g can be obtained, as shown in the inset of Figure 4. The uncertainty is estimated about 1%–5% which depends on the data points. The variation of, E_g with x can be fitted by the equation $E_g = 4.05 + 1.34x - 1.97x^2$ in the whole doping range $x = 0.1$–0.9.

It is clear that, E_g increases at first then decreases with the doping concentration x. The increase in, E_g can be analyzed by the Burstein-Moss effect due to the enhanced carrier concentration (Moss and Smoluchowski, 1952; Burstein, 1954). When increase x further ($x > 0.3$), however, E_g decreases from 4.25 to 3.66 eV. This is understandable, since, E_g of SSO is 4.27 eV while that of SVO is 3.5 eV. Consequently, the impurity bands that consisted of the V 3d states act as extra valence bands in addition to the O 2p band as a result of substitutional doping V into SSO. Then the valence band edge moves closer to the bottom of the conduction band. The introduction of V ion into the band gap of SSO accounts for the narrowing band gap (Dakhel, 2012).

Figure 5 shows the z-scan measurement results for the SSVO films. It seems that the nonlinearity responses vary in different ways along with the doping concentration at point $x = 0.5$. For

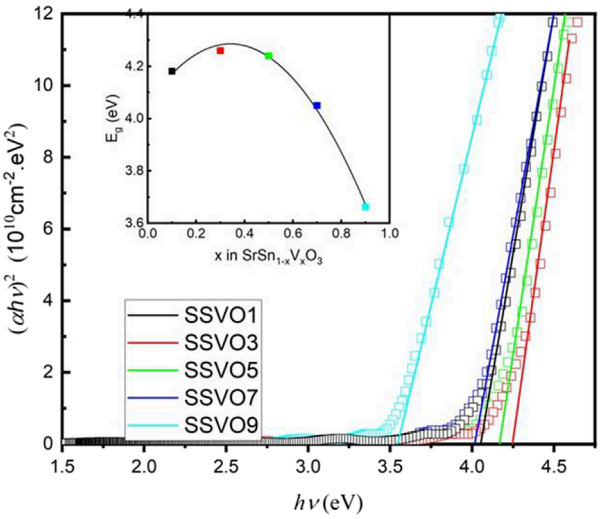

FIGURE 4
Plots of $(\alpha h\nu)^2$ *versus* $h\nu$ for the SSVO films. Inset: Extracted, E_g values as a function of V content in SSVO films.

comparative analysis, Figure 5 (a1) and (b1) show the results for SSVO1, SSVO3, and SSVO5, and Figure 5 (a2) and (b2) show the results for SSVO5, SSVO7, and SSVO9.

The OA data, as shown in Figure 5 (a1) and 5 (a2), demonstrate peaks at z = 0, indicating that the existence of saturated absorption β

10.3389/fmats.2023.1341006

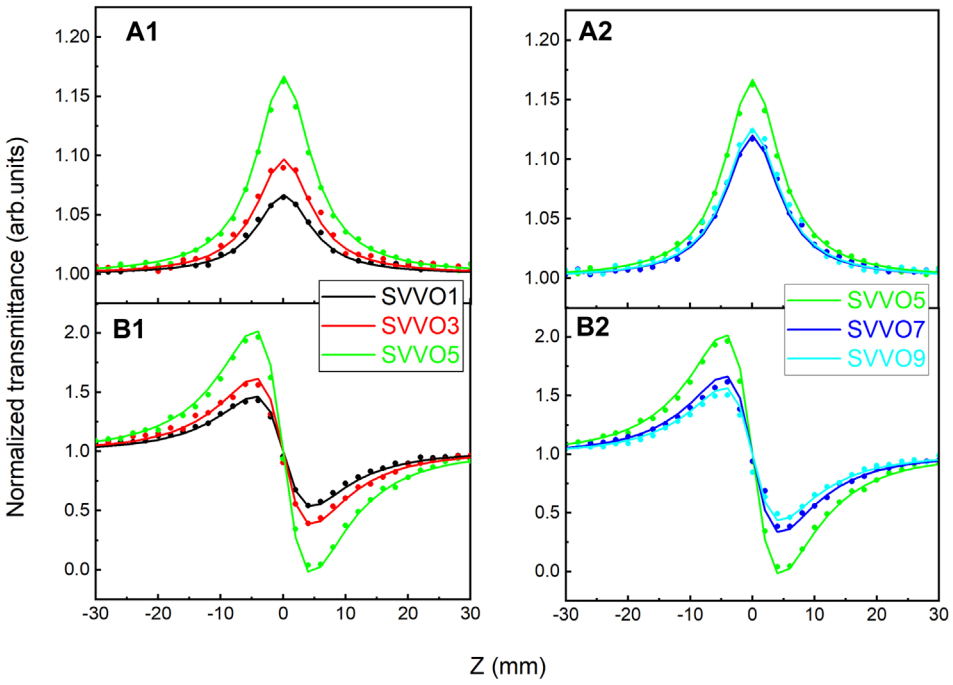

FIGURE 5
OA (a1,a2) and CA (b1,b2) z-scan results for the SSVO films.

TABLE 2 The nonlinear optical parameters of the samples.

Sample	SSVO1	SSVO3	SSVO5	SSVO7	SSVO9
β (10^{-8} m/W)	3.63	5.40	7.66	5.91	5.93
Im$\chi^{(3)}$ (10^{-9}esu)	1.0	1.48	2.10	1.61	1.63
n_2 (10^{-13}m^2/W)	0.98	1.30	2.01	1.38	1.33
Re$\chi^{(3)}$ (10^{-8}esu)	6.61	8.64	13.56	9.31	8.97

and negative imaginary part of the third-order susceptibility Im$\chi^{(3)}$. The CA data, as shown in Figure 5 (b1) and 5 (b2), display a peak-valley shape, which means a pre-focal maximum followed by a post-focal minimum for all samples. This configuration manifests the negative nonlinear refractive index n_2 and real part of the third-order susceptibility Re$\chi^{(3)}$. Given the OA and CA data, it seems that the V doping concentration x has promising effect on Im$\chi^{(3)}$ and Re$\chi^{(3)}$ significantly.

By using the normalized transmittance at OA peak, β and Im$\chi^{(3)}$ can be calculated through the following equation (Liu et al., 2019),

$$T_{OA}(z) = 1 - \frac{\beta I_0 L_{eff}}{2\sqrt{2}(1+x^2)},$$

and $\mathrm{Im}\chi^{(3)}(esu) = \frac{\lambda c n_0^2}{480\pi^3}\beta(m/W)$,

where L_{eff} is the effective thickness of the film, $x = z/z_R$, and $z_R = \pi\omega_0{}^2/\lambda$ is the Rayleigh length of the beam, λ, c, n_0 are incident light wavelength, speed of light in vacuum, and linear refractive index, respectively. The value of n_0 can be obtained from Refs. (Ismail and Desouky, 2023; Ghebouli et al., 2009)

The CA data can be fitted using the following equation (Liu et al., 2019),

$$T_{CA}(z) = 1 - \frac{8\pi x n_2 I_0 L_{eff}}{\lambda(x^2+9)(x^2+1)},$$

n_2 and Re$\chi^{(3)}$ are related through

$$\mathrm{Re}\chi^{(3)}(esu) = \frac{cn_0^2}{120\pi^2} n_2(m^2/W).$$

The obtained values of β, Im$\chi^{(3)}$, n_2, and Re$\chi^{(3)}$ for the SSVO films are listed in Table 2. The relative uncertainty in the values is estimated to be about 10%, which is typical of z-scan measurements.

The variation of $\chi^{(3)}$ with the doping concentration x is plotted in Figure 6 using a spline connection. With the increase of x, the value of $\chi^{(3)}$ initially increases and then decreases, and the maximum appears at $x = 0.5$ (SSVO5).

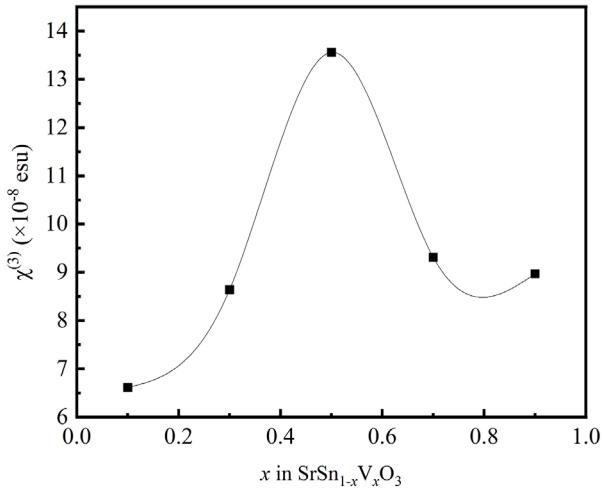

FIGURE 6
Variation of $\chi^{(3)}$ with V content in SSVO films.

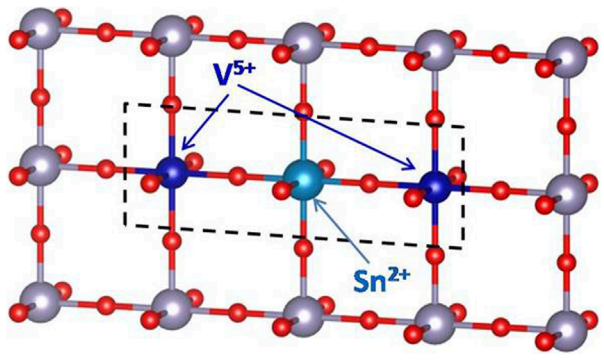

FIGURE 7
Ball-and-stick illustration of the $V^{5+}Sn^{3+}$ complex sketched with dashed lines. Unlabelled atoms are Sn^{4+} (gray) and O (red).

As for metal oxides, the metal-oxygen covalent bond length plays an important role for the third-order optical nonlinearity. With the doping of V, the lattice volume shrinks, which is demonstrated by XRD data (Figure 2). According to the bond-orbital theory (Lines, 1991), the shorter metal-oxygen length, the larger nonlinear optical responses. The Sn-O bond length in $SrSnO_3$ is 2.057Å, and the V-O bond length in $SrVO_3$ is 1.950 Å (Inoue et al., 1998; Zhang et al., 2007). It is understandable that the bond length decreases along with the substitution of Sn site of $SrSnO_3$ with V ions. As a result, the value of $\chi^{(3)}$ for the prepared $SrSn_{1-x}V_xO_3$ films increases with x in the range of $x = 0.1–0.5$.

On the other hand, in the case of low doping concentration $x \leq 0.5$, the valence state of most of the doping V ions is +5, as shown in Figures 3C,F. Since the chemical state of Sr ions shows no measurable change resulted from V doping, V^{5+} substitutions locally induce the reduction of Sn^{4+} to Sn^{2+} as follows:

$$V_2O_5 + SnO_2 \xrightarrow{3SnO_2} 2V_{Sn}^{\bullet} + Sn_{Sn}'' + 6O_O + \frac{1}{2}O_2,$$

$$Sn^{4+} + 2e \rightarrow Sn^{2+}.$$

The resulting $V^{5+}Sn^{2+}V^{5+}$ complex, as shown in Figure 7, gives rise to dipole-like cluster with the electrons localized. The localized electrons contribute significantly to the enhancement of the permittivity and optical nonlinearity (Hu et al., 2013). As is known, the third-order optical nonlinearity of materials with localized electrons can be enhanced by artificially confining the electrons in localized regions (Banfi et al., 1998). It can be considered that the complex-related effect plays the main role in the optical nonlinearity enhancement. However, with further increase of the doping concentration $x > 0.5$, the valence state of V ions gradually changes to +4 (as shown in Figure 3C), and the dipole-like cluster disappears, which leads to the decrease of the nonlinear optical responses. It seems that this complex-related effect plays the main role in the optical nonlinearity for $x > 0.5$.

4 Conclusion

In summary, we have demonstrated an experimental method for the modulation of the band gap and enhancement of the third-order optical nonlinearity in $SrSn_{1-x}V_xO_3$ films by adjusting the doping concentration x. In the range of $x = 0.1–0.9$, the optical bandgap in eV can be expressed as $E_g = 4.05 + 1.34x - 1.97x^2$. Both the metal-oxygen covalent bond and localized dipole-like cluster contribute to the enhancement of the third-order nonlinear optical responses at low doping concentrations $x \leq 0.5$. With increasing the doping concentration further, however, the value of $\chi^{(3)}$ decreases as a result of the disappearance of $V^{5+}Sn^{2+}V^{5+}$complex due to the changes of V and Sn chemical states.

Data availability statement

The original contributions presented in the study are included in the article/Supplementary material, further inquiries can be directed to the corresponding author.

Author contributions

ZH: Data curation, Writing–original draft. QM: Formal Analysis, Writing–review and editing. DW: Investigation, Software, Writing–review and editing. RZ: Software, Investigation, Writing–review and editing. RN: Investigation, Software, Writing–review and editing. WW: Supervision, Writing–review and editing.

Funding

The author(s) declare financial support was received for the research, authorship, and/or publication of this article. This work was supported by the National Natural Science Foundation of China

(No. 10704065) and the Graduate Innovation Foundation of Yantai University (No. GGIFYTU2315).

Conflict of interest

The authors declare that the research was conducted in the absence of any commercial or financial relationships that could be construed as a potential conflict of interest.

Publisher's note

All claims expressed in this article are solely those of the authors and do not necessarily represent those of their affiliated organizations, or those of the publisher, the editors and the reviewers. Any product that may be evaluated in this article, or claim that may be made by its manufacturer, is not guaranteed or endorsed by the publisher.

References

Absike, H., Baaalla, N., Attou, L., Labrim, H., Hartiti, B., and Ez-zahraouy, H. (2022). Theoretical investigations of structural, electronic, optical and thermoelectric properties of oxide halide perovskite $ACoO_3$ (A=Nd, Pr or La). *Solid State Commun.* 345, 114684. doi:10.1016/j.ssc.2022.114684

Ando, M., Kadono, K., Haruta, M., Sakaguchi, T., and Miya, M. (1995). Large third-order optical nonlinearities in transition-metal oxides. *Nature* 374, 625–627. doi:10.1038/374625a0

Atuchin, V. V., Ayupov, B. M., Kochubey, V. A., Pokrovsky, L. D., Ramana, C. V., and Rumiantsev, Y. M. (2008). Optical properties of textured V_2O_5/Si thin films deposited by reactive magnetron sputtering. *Opt. Mat.* 30, 1145–1148. doi:10.1016/j.optmat.2007.05.040

Bahae, M. S., Said, A. A., Wei, T. H., Hagan, D. J., and Stryland, E. W. V. (1990). Sensitive measurement of optical nonlinearities using a single beam. *IEEE J. Quantum Electron.* 26, 760–769. doi:10.1109/3.53394

Banfi, G., Degiorgio, V., and Ricard, D. (1998). Nonlinear optical properties of semiconductor nanocrystals. *Adv. Phys.* 47, 447–510. doi:10.1080/000187398243537

Benaissa, M., Sigle, W., Benabdallah, I., Elafandy, R. T., Ng, T. K., and Van Aken, P. A. (2021). Optical properties of freestanding GaN nanomembranes using monochromated valence-EELS. *Mat. Sci. Eng. b-adv.* 272, 115333. doi:10.1016/j.mseb.2021.115333

Biesinger, M. C., Lau, L. W. M., Gerson, A. R., and Smart, R. S. C. (2010). Resolving surface chemical states in XPS analysis of first row transition metals, oxides and hydroxides: Sc, Ti, V, Cu and Zn. *Appl. Surf. Sci.* 257, 887–898. doi:10.1016/j.apsusc.2010.07.086

Burstein, E. (1954). Anomalous optical absorption limit in InSb. *Phys. Rev.* 93, 632–633. doi:10.1103/PhysRev.93.632

Dakhel, A. A. (2012). Structural and optoelectronic properties of Zn-incorporated CdO films prepared by sol–gel method. *J. Alloys Compd.* 539, 26–31. doi:10.1016/j.jallcom.2012.05.117

Gao, D. S., Gao, X. D., Wu, Y. Q., Zhang, T. T., Yang, J. N., Li, X. M., et al. (2019). Co-doped $SrSnO_3$ epitaxial thin films on MgO with tunable band gap and room-temperature ferromagnetism. *Phys. E* 109, 101–106. doi:10.1016/j.physe.2019.01.010

Gao, X. D., Hu, X. M., Li, X., Gu, Z., Ying, S., Wu, Y., et al. (2016). Microstructure and band gap modulation of $SrSn_{1-x}Co_xO_3$ epitaxial thin films via pulsed laser deposition. *Acta. phys.-chim. Sin.* 32, 828–833. doi:10.3866/PKU.WHXB201603013

Ghebouli, B., Ghebouli, M. A., Chihi, T., Fatmi, M., Boucetta, S., and Reffas, M. (2009). First-principles study of structural, elastic, electronic and optical properties of SrMO3 (M = Ti and Sn). *Solid State Commun.* 149, 2244–2249. doi:10.1016/j.ssc.2009.09.001

Guo, P., An, M., Shu, Y., Peng, X., Han, Y., Hu, H., et al. (2022). Nonlinear photonics device based on double perovskite oxide Ba_2LaTaO_6 for ultrafast laser generation. *Opt. Laser Technol.* 155, 108334. doi:10.1016/j.optlastec.2022.108334

Hu, W., Liu, Y., Withers, R. L., Frankcombe, T. J., Norén, L., Snashall, A., et al. (2013). Electron-pinned defect-dipoles for high-performance colossal permittivity materials. *Nat. Mat.* 12, 821–826. doi:10.1038/nmat3691

Inoue, I. H., Goto, O., Makino, H., Hussey, N. E., and Ishikawa, M. (1998). Bandwidth control in a perovskite-type $3d^1$-correlated metal $Ca_{1-x}Sr_xVO_3$. I. Evolution of the electronic properties and effective mass. *Phys. Rev. B* 58, 4372–4383. doi:10.1103/PhysRevB.58.4372

Ismail, A. M., and Desouky, F. G.El. (2023). Facile assembly of fexible quaternary SnO_2/$SrSnO_3$/Fe_3O_4/PVDF nano-composites with tunable optical, electrical, and magnetic properties for promising magneto-optoelectronic applications. *Sci. Rep.* 13, 4997. doi:10.1038/s41598-023-32090-w

Leal-Perez, J. E., Flores-Valenzuela, J., Almaral-Sánchez, J. L., Herrera-Basurto, R., González-Hernández, J., Auciello, O., et al. (2022). Cole-Cole analysis and optoelectronic properties, using VEELS, of KNNS ferroelectric ceramics. *Mat. Today Commun.* 33, 104781. doi:10.1016/j.mtcomm.2022.104781

Li, K., Gao, Q., Zhao, L., and Liu, Q. (2020). Electrical and optical properties of Nb doped $SrSnO_3$ epitaxial films deposited by pulsed laser deposition. *Nanoscale Res. Lett.* 15, 164. doi:10.1186/s11671-020-03390-1

Lines, M. E. (1991). Influence of d orbitals on the nonlinear optical response of transparent transition-metal oxides. *Phys. Rev. B* 43, 11978–11990. doi:10.1103/PhysRevB.43.11978

Liu, G., Dai, S., Zhu, B., Li, P., Wu, Z., and Gu, Y. (2019). Third-order nonlinear optical properties of MoSe2/graphene composite materials. *Opt. Laser Technol.* 120, 105746. doi:10.1016/j.optlastec.2019.105746

Liu, Q., Jin, F., Gao, G., and Wang, W. (2017). Ta doped $SrSnO_3$ epitaxial films as transparent conductive oxide. *J. Alloy. Compd.* 717, 62–68. doi:10.1016/j.jallcom.2017.05.080

Liu, Q., Li, H., Li, B., Wang, W., Liu, Q., Zhang, Y., et al. (2014). Structure and band gap engineering of Fe-doped $SrSnO_3$ epitaxial films. *EPL* 108, 37003. doi:10.1209/0295-5075/108/37003

Makino, H., Inoue, I. H., Rozenberg, M. J., Hase, I., Aiura, Y., and Onari, S. (1998). Bandwidth control in a perovskite-type $3d^1$-correlated metal $Ca_{1-x}Sr_xVO_3$. II. Optical spectroscopy. *Phys. Rev. B* 58, 4384–4393. doi:10.1103/physrevb.58.4384

Manorama, S. V., Gopal Reddy, C. V., and Rao, V. J. (2001). X-ray photoelectron spectroscopic studies of noble metal-incorporated $BaSnO_3$ based gas sensors. *Appl. Surf. Sci.* 174, 93–105. doi:10.1016/S0169-4332(00)00914-4

Moss, T. S., and Smoluchowski, R. (1952). Photoconductivity in the elements. *Phys. Today* 7, 18. doi:10.1063/1.3061511

Oka, H., Okada, Y., Kaminaga, K., Oka, D., Hitosugi, T., and Fukumura, T. (2020). Width-induced metal–insulator transition in $SrVO_3$ lateral nanowires spontaneously formed on the ultrathin film. *Appl. Phys. Lett.* 117, 051603. doi:10.1063/5.0018240

Pattipaka, S., Joseph, A., Bharti, G. P., Raju, K. C. J., Khare, A., and Pamu, D. (2019). Thickness-dependent microwave dielectric and nonlinear optical properties of $Bi_{0.5}Na_{0.5}TiO_3$ thin films. *Appl. Surf. Sci.* 488, 391–403. doi:10.1016/j.apsusc.2019.05.264

Sakhya, P., Rai, D. P., Sheikh, Md. S., Mukherjee, M., Dutta, A., and Sinha, T. P. (2017). Origin of the optical anisotropy and the electronic structure of Ru-based double perovskite oxides: DFT and XPS studies. *RSC Adv.* 7, 43531–43539. doi:10.1039/C7RA07712B

Sharma, N., Shaju, K. M., Subba Rao, G. V., and Chowdari, B. V. R. (2005). Anodic behaviour and X-ray photoelectron spectroscopy of ternary tin oxides. *J. Power Sources* 139, 250–260. doi:10.1016/j.jpowsour.2004.06.057

Shereef, A., Aleena, P. A., Kunjumon, J., Jose, A. K., Thomas, S. A., Tomy, M., et al. (2023). Third order nonlinear optical properties and electrochemical performance of La_2CoMnO_6 double perovskite. *Mat. Sci. Eng. b-adv.* 289, 116262. doi:10.1016/j.mseb.2023.116262

Silversmit, G., Depla, D., Poelman, H., Marin, G. B., and Gryse, R.De. (2004). Determination of the V2p XPS binding energies for different vanadium oxidation states (V^{5+} to V^{0+}). *J. Electron Spectrosc. Relat. Phenom.* 135, 167–175. doi:10.1016/j.elspec.2004.03.004

Tauc, J., Grigorovici, R., and Vancu, A. (1966). Optical properties and electronic structure of amorphous germanium. *Phys. Stat. Sol.* 15, 627–637. doi:10.1002/pssb.19660150224

Wang, D., Niu, R., Cui, L., and Wang, W. (2023). Effect of Ba/Sr ratio on the nonlinear optical properties of $Ba_{1-x}Sr_xTiO_3$ (x = 0.1–0.9) thin films. *Chin. Opt. Lett.* 21, 041601. doi:10.3788/COL202321.041601

Zhang, W., Tang, J., and Ye, J. (2007). Structural, photocatalytic, and photophysical properties of perovskite $MSnO_3$ (M = Ca, Sr, and Ba) photocatalysts. *J. Mat. Res.* 22, 1859–1871. doi:10.1557/jmr.2007.0259

Zhang, W. F., Tang, J., and Ye, J. (2006). Photoluminescence and photocatalytic properties of $SrSnO_3$ perovskite. *Chem. Phys. Lett.* 418, 174–178. doi:10.1016/j.cplett.2005.10.122